Unraveling the Capacitive Charge Storage Mechanism of Nitrogen-Doped Porous Carbons by EQCM and ssNMR

En Zhang, Yih-Chyng Wu, Hui Shao, Vytautas Klimavicius, Hanyue Zhang, Pierre-Louis Taberna, Julia Grothe, Gerd Buntkowsky, Fei Xu, Patrice Simon, et al.

Unravelling the capacitive charge storage mechanism of nitrogen doped porous carbons by EQCM and ssNMR

En Zhang[a], Yih-Chyng Wu[b,c], Hui Shao[b,c], Vytautas Klimavicius[d,e], Hanyue Zhang[a], Pierre-Louis Taberna[b], Julia Grothe[a], Gerd Buntkowsky[e], Fei Xu[a*], Patrice Simon[b,c,*] and Stefan Kaskel[a,f*]

[a]Inorganic Chemistry I, Technische Universität Dresden, Bergstraße 66, 01069 Dresden, Germany

[b]Université Paul Sabatier, CIRIMAT UMR CNRS 5085, 31062 Toulouse, France

[c]Réseau sur le Stockage Electrochimique de l'Energie (RS2E), FR CNRS 3459, France

[d]Institute of Chemical Physics, Vilnius University, Sauletekio av. 3, LT-10257 Vilnius, Lithuania

[e]Technical University Darmstadt, Eduard-Zintl-Institute for Inorganic and Physical Chemistry, Alarich-Weiss-Straße 8, 64287 Darmstadt, Germany

[f]Fraunhofer Institute for Material and Beam Technology (IWS), Winterbergstraße 28, 01277 Dresden,Germany

E-mail: feixu@nwpu.edu.cn; simon@chimie.ups-tlse.fr; stefan.kaskel@tu-dresden.de

Abstract : Fundamental understanding of ion electroadsorption processes in porous electrodes for energy storage on a molecular level is of high importance to propose guidelines for rational design of next generation energy storage devices like electric double layer capacitors (EDLCs). Porous carbons functionalized by heteroatoms such as nitrogen show enhanced capacitive performance but the underlying mechanism is still elusive, due to the lack of reliable tools to precisely identify multiple N species and establish clear structure property relations. Here, we use advanced analytical techniques such as low temperature solid-state NMR (ssNMR) and electrochemical quartz crystal microbalance (EQCM) to relate the complex nitrogen functionalities in porous carbons to the charging mechanisms and capacitive performance. For the first time it is demonstrated in a molecular level that N-doping strongly influences the electroadsorption mechanism in EDLCs. Without N-doping, anion (SO_4^{2-}) adsorption/desorption dominates the charging mechanism, whereas after doping Li^+ electroadsorption plays a key role. With the help of EQCM, it is demonstrated that SO_4^{2-} is strongly immobilized on the N-doped surface, leaving Li^+ as the main charge carrier. The smaller size and higher concentration of Li^+ compared to SO_4^{2-} benefit a higher capacitance. Amine/amide N is responsible for high capacitance but surprisingly the pyridinic, pyrrolic and graphitic N groups are proved to have no significant influence in the electrochemical behaviour in 1M Li_2SO_4 electrolyte. 2D ^1H-^{15}N NMR spectroscopy is capable of enabling the identification of pyrrolic and pyridinium N, and the conversion from pyridinium to pyrrolic N gives rise to slightly decreased capacitance. This work not only demonstrates ssNMR as a powerful tool for surface chemistry characterization of electrode materials, but also uncovers the related charging mechanism by EQCM, paving the way towards a comprehensive picture of EDLC chemistry and helping sophisticatedly designing and screening of promising electrode materials.

Introduction

EDLCs have been receiving significant attention in the last decades, not only for their excellent energy storage performance featuring high power density, long cycle life and low maintenance cost[1-4], but also for their emerging new application potential in advanced iontronic devices such as CAPode[5] and G-Cap[6]. Since EDLCs store energy by nanoconfined accumulation of ions on the electrode surface, the electrode surface texture and chemical composition significantly influence the capacitance and electrode-electrolyte interaction and consequently their charging mechanisms[7-8].

Nitrogen doping is a versatile approach for

surface modification and structural engineering[9-11]. Due to the electronegativity difference and charge polarization, N-doped carbons usually show enhanced hydrophilicity and stronger guest-host interaction[12]. Meanwhile, nitrogen with an extra electron can improve the electrical conductivity of the carbon framework and itself can also be used as electroactive site contributing pseudocapacitance[13-14]. Therefore, nitrogen doping plays a pivotal role in catalysis and its support, gas adsorption and energy storage and conversion[15-19]. However, a molecular understanding of the wide variety of N configurations influencing the performance is still lacking and remains a subject of dispute. For instance, in EDLCs, controversial conclusions regarding the clarification of the atomic composition and their role in electrochemical performance on the origin of pseudocapacitance from various N species and their role in different electrolyte systems has been obtained in the last few years[20-28]. The greatest challenge is that it is almost impossible to unambiguously differentiate the various N species. Although X-ray core-level spectroscopy, such as X-ray photoelectron spectroscopy (XPS) can provide element-specific quantitative analysis[29-31], the accuracy of the interpretation is mainly based on the subjective recognition of the investigated materials and heavily depends on the deconvolution procedure. Not to mention several N moieties overlap over a very narrow binding energy range, impeding the unambiguous assignment of the nitrogen functional groups[25, 32-33].

In this context, NMR spectroscopy emerged as an ideal analytical technique for unmasking the structural and chemical composition with respect to its ultra-sensitivity to the local environment and diverse forms of analysis methods, ranging from 1D NMR[34-35] to 2D correlation NMR[36-37] and advanced spectroscopy such as dynamic nuclear polarization NMR[38] and pulsed field gradient NMR spectroscopy[37, 39-44]. Grey's group and their collaborators have published some pioneer works, where they used in-situ NMR to reveal the EDL structure in nanoporous carbon, possible charging mechanism and ion dynamics in EDLCs[45-48]. However the influence of carbon surface chemistry is rarely discussed but of vital importance (e.g. why N-doped carbon can enhance the capacitance?) for drawing a comprehensive picture of interfacial interaction, which is still an uncharted area.

Meanwhile, storing energy is a highly dynamic process. Complementary in-situ techniques capable of providing real-time information are necessary to fully uncover the mystery of the charging/discharging mechanism. Electrochemical quartz crystal microbalance (EQCM) is an effective technique to probe electrode-electrolyte interaction. It is found that depending on the pore size, the charging mechanism for different bias is distinctive. For carbon electrode with 1 nm pore width, a positive bias only adsorbs cations while a negative bias involves both cations and anions[49]. EQCM is also capable of studying ion dynamics and interfacial capacitance on a single layer graphene[50-51]. It should be mentioned that surface chemistry is a key aspect for the electrode-electrolyte interaction, directly influencing the electrode capacitance, ion flux, ion kinetics and the interface at the electrodes, especially for the N-doped materials[9-11]. However, less attention has been paid to the influence of electrode surface chemistry on the charging mechanism.

Consequently, exploring reliable techniques to precisely identify the N moieties and meanwhile unravelling the real-time ion dynamics and interfacial interactions on N doped surface, are of great significance and highly desirable, which could offer opportunity for supplementing or even transcending the limitations associated with the current methodologies. Herein, we applied ^{15}N enriched urea for carbon functionalization and combined XPS, ssNMR and in-situ EQCM studies to obtain a clear identification of nitrogen species and to unravel the storage mechanism. An unambiguous assignment of the nitrogen species was realized, contributing to the clarification of the influences of nitrogen doping in a molecular level. In particular, amine groups lead to an anion immobilization shifting the predominant species for electroadsorption from anions to cations.

Results and discussion

Our strategy starts from a well etsablished EDLC reference material, the commercially available activated carbon YP50F. For successful functionalization it was firstly oxidized by nitric acid with subsequent hydrothermal treatment with ^{15}N enriched urea for better NMR analysis. The obtained sample was designated as NYP-HT. A hydrothermal treatment at low temperature (453 K) is advantageous for maintaining the high temperature unstable N species (such as amino groups) and a post-treatment is believed to largely maintain the morphology and pore structure of the original YP50F. As can be seen in nitrogen physisorption (Figure 1c), YP50F and NYP-HT both show type I isotherms with a small hysteresis, indicative of the predominant microporosity and minor mesoporosity. There is almost no decrease in porosity after the doping process. Pore size distribution also indicates insignificant changes in their porosity (Figure S1). The slightly decreased porosity for NYP-HT is actually consistent with the anchored nitrogen content of 4.8 wt% (Table 1). From XPS, NYP-HT shows a comparable N amount (5.2 at%) to that of the elemental analysis,

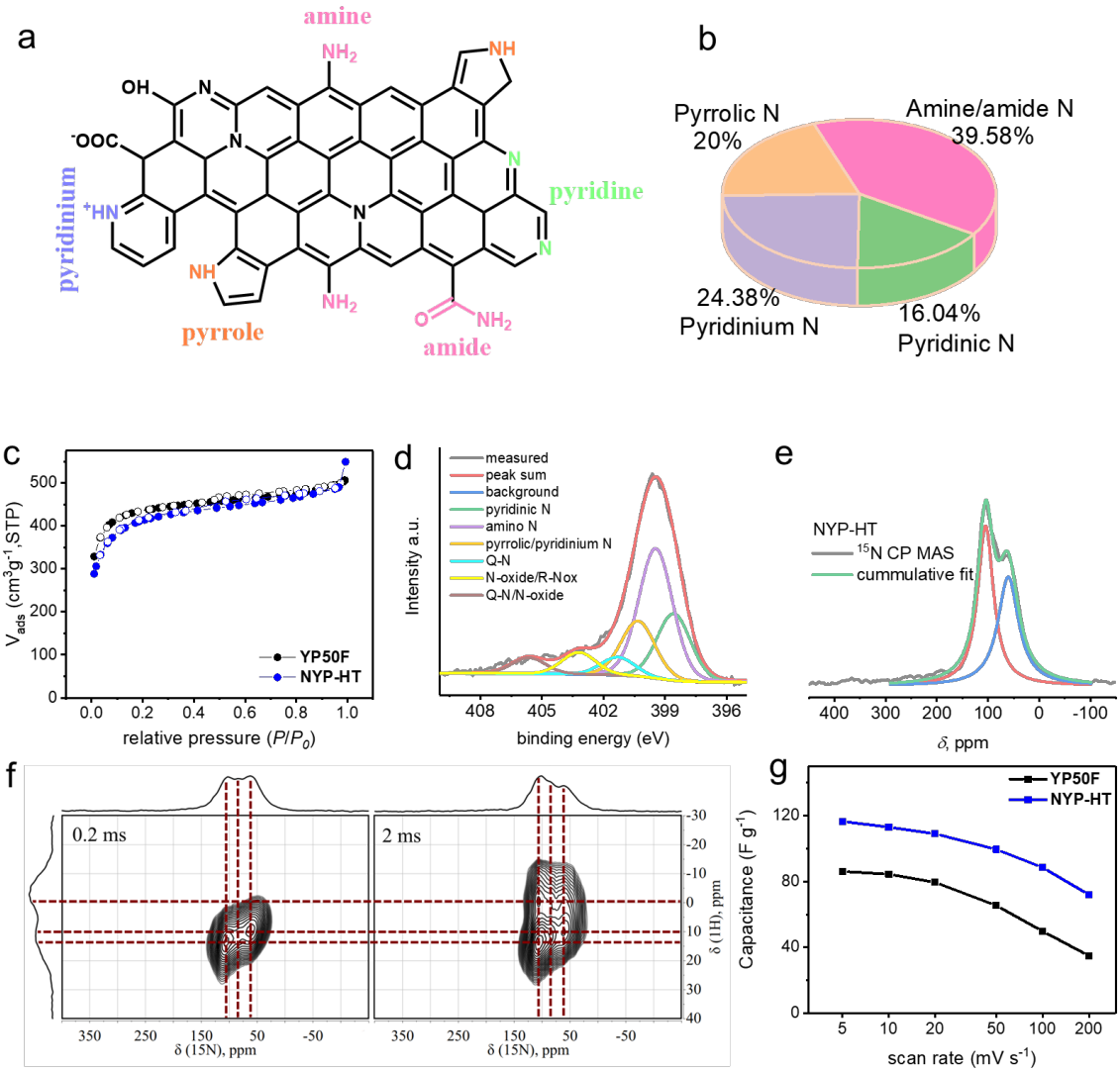

Figure 1. Porosity, chemical and electrochemical characterization of YP50F and NYP-HT. a) a schematic introduction of possible N species of N-doped carbons. b) composition of various N moieties in the NYP-HT. To note, the amount is based on the combined analysis of XPS and NMR and is more qualitatively based number for a better understanding. c) N_2 physisorption at 77K, d) XPS for NYP-HT, e) MAS NMR for NYP-HT, f) ^{1}H-^{15}N 2D NMR for NYP-HT, g) rate performance.

confirming a homogeneous distribution of the N species from bulk to surface (showcased in Figure 1a and 1b).

XPS results gives useful qualitative/quantitative information on the changing concentration of N species resulting from different treatments. The analysed results are referred to the available literatures[29-31, 52-53] and will be further evaluated by low temperature NMR spectroscopy. NYP-HT contains predominantly amide and amine N (-NH_2) species (46 at%) resulting from the low hydrothermal temperature of 453 K. The residual N species have relatively low amounts up to 16 at% (detailed in Table S1). Cross polarization magic angle spinning (CPMAS) NMR spectroscopy is also used for mapping the chemical structure of ^{15}N labelled N-doped carbon (Figure 1e). In contrast to traditional characterization methods like XPS, where various signals should be differentiated within only a few eV differences, NMR spectra show a wider spread of chemical shifts for various N species[54-55]. Although only a few literatures try to clarify the N species by NMR, together with theoretical simulation, the NMR peak assignment is explicit[55-58]. NYP-HT has mainly two peaks located at 55 ppm and 105 ppm corresponding to amine/amide N and cyclic N with proton (like pyrrolic/pyridinium N), respectively[55-56]. This part is consistent with the XPS result. Noteworthy, the differentiation of pyrrolic and other protonated N (like pyridinium N) is rarely reported in EDLCs, and generally only pyrrolic N was mentioned to clarify the electrochemical performance neglecting pyridinium N[59-61], which can lead to a

Table 1. Porosity and N content of various carbon materials.

Materials	SSA ($m^2 g^{-1}$)[a]	PV($cm^3 g^{-1}$)[b]	N[c] (wt%)
YP50F	1746	0.74	0.30
NYP-HT	1537	0.70	4.80
NYP-HT-Ar	1441	0.64	4.56
NYP-HT-H_2	1576	0.70	3.73

[a] specific surface area based on a BET method. [b] cumulative pore volume based on a QSDFT method.

[c] N content from elemental analysis.

misunderstanding. The reason for the difficult characterization is that the energy level for these two species is too similar, leading to strong overlap in the spectrum envelop. This challenge unfortunately also remains for 1D CPMAS spectroscopy. However, when we have a close look at these two species, aside from N there is always a directly bonded H in these two species, which have a chemical difference of about 10 ppm in a 2D ^{1}H-^{15}N NMR[55], large enough for discrimination of pyridinium N and pyrrolic N. The proton signal locates at about 10 ppm for pyrrolic N and for pyridinium N at about 0 ppm[55]. In NYP-HT (Figure 1f), two peaks are evenly distributed at 0 ppm and 10 ppm, meaning NYP-HT has a comparable amount of pyrrolic and pyridinium N.

Moreover, the surface hydrophilicity/polarity of NYP-HT is totally changed after doping. In the water physisorption isotherm (Figure S2), YP50F has almost no uptake at low relative pressure, indicative of the very weak interaction between water and hydrophobic carbon surface[12, 31]. However, NYP-HT exhibits much enhanced water uptake below p/p_0 = 0.4, almost 4 times as much as YP50F. Obviously, the N functional groups can improve the surface polarity and enhance the interaction between carbon pore wall and water molecules, which is beneficial for aqueous electrolyte-based energy storage system[7, 62]. As expected, when these carbons are used as electrode materials for supercapacitors in 1 M Li_2SO_4 electrolyte (Figure 1g), both carbons show almost ideal rectangular shapes, indicating their good capacitive performance (Figure S3). However, NYP-HT has a much higher capacity (116 F g^{-1} at 5 mV s^{-1}) compared to the original YP50F (86 F g^{-1} at 5 mV s^{-1}). In impedance spectroscopy (Figure S4), the plots for YP50F and NYP-HT exhibit a typical transmission line behaviour, as expected for a porous carbon: a high frequency intercept (on the left part of abscissa), related to the bulk electrolyte resistance, which is the same for both carbons; a vertical line, at low frequency (right part of abscissa), related to the capacitive behaviour of each carbon; in-between (middle range frequency) a 45° linear increase of the impedance is observed, linked to in-pore ionic resistance. In accordance with the cyclic voltammograms, the low frequency impedance is smaller for NYP-HT as the capacitance is higher. Interestingly, the 45° slope region is larger for YP50F than that for NYP-HP, in line with the higher hydrophilicity observed for NYP-HP (electrode thickness was maintained at 100μm). Indeed, higher hydrophilicity leads in turn to a higher electrochemically active surface area in an aqueous-based electrolyte. This can partially clarify why NYP-HT has a higher capacitance than YP50F. Considering the fact that there is almost no change in the porosity, the extreme difference of the two carbons should be attributed to their distinct surface chemistry. This means a suitable amount and appropriate species of N functional groups are of vital importance for the capacitive performance in an aqueous-based electrolyte.

To further clarify the influences of different N species on the capacitive behaviour and on the charging mechanism, NYP-HT is treated at 773 K under Ar (NYP-HT-Ar) and H_2 (NYP-HT-H_2) atmosphere to remove the unstable functional groups. After the heat treatments, texturally, N_2 physisorption isotherm and pore size distribution have almost no change (Figure 2a and Figure S5) for both carbons, indicative of the well-maintained porosity. Chemically, NYP-HT-Ar has slightly decreased N content to 4.6 wt% and NYP-HT-H_2 to 3.7 wt% (from 4.8 wt%). It is worth noting that in XPS the –NH_2 amount decreased from 46% to 23% for NYP-HT-Ar (Figure 2b). However, in 1D ^{15}N CP NMR spectra (Figure 2c), it decreases only to 45%. Again, as mentioned before, XPS results can not clearly distinguish species within very small energy range, it is accepted here that the NMR results are more sensible to show the general trend. The XPS data are used as a complementary tool for this species for better consistency. The following discussion is based on a qualitative analysis (calculating pyridinic N content from XPS and others from NMR). The 1D ^{15}N CP MAS NMR spectra for NYP-HT-H_2 show a similar shape to that for NYP-HT-Ar (Figure 2f). The most distinctive difference is that NYP-HT-Ar has only slightly decreased intensity for the -NH_2 group (at 55 ppm) while NYP-HT-H_2 has strongly decreased -NH_2 content (23%). In addition, a broad shoulder is

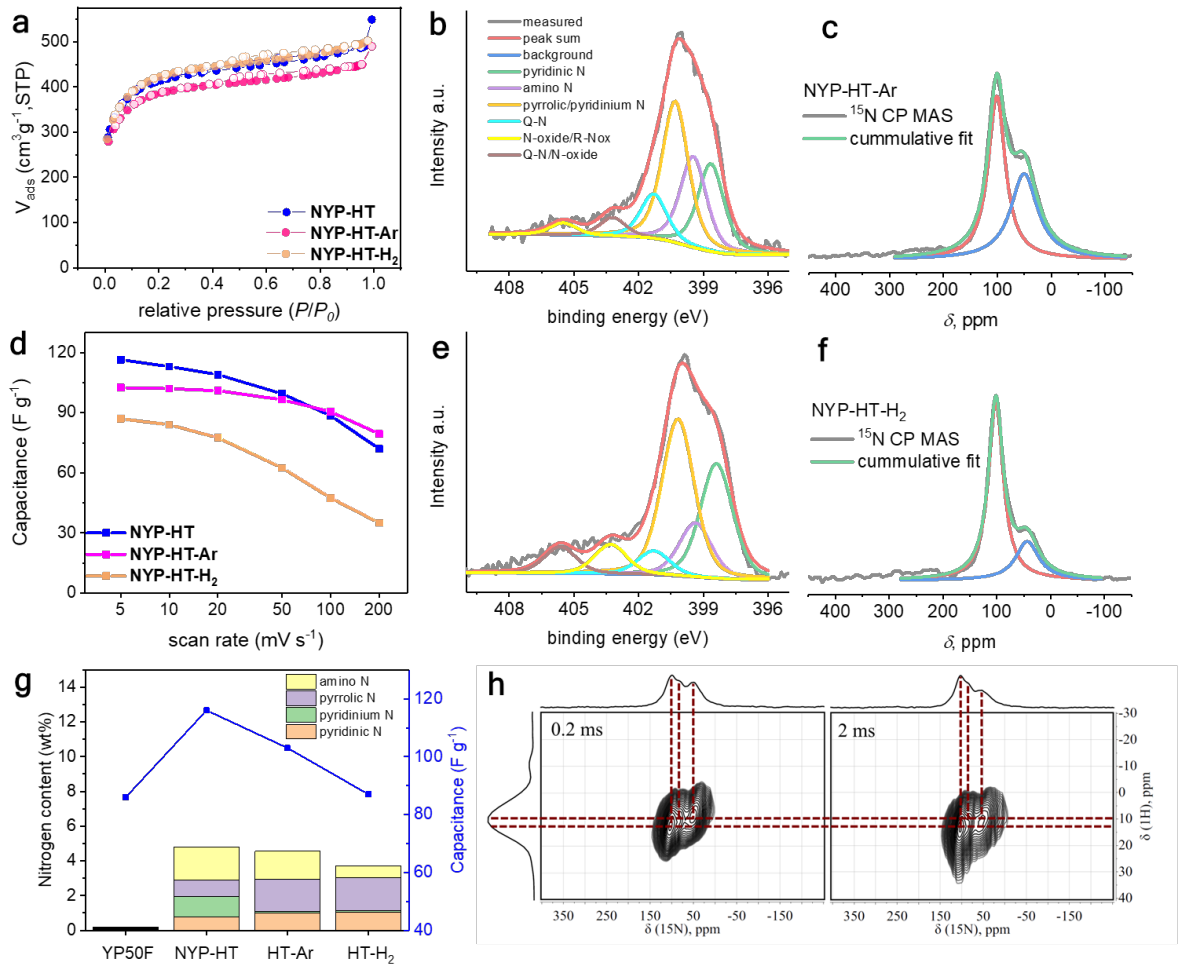

Figure 2. Porosity, chemical and electrochemical characterization of NYP-HT-Ar and NYP-HT-H_2. a) N_2 physisorption at 77K, b) XPS for NYP-HT-Ar, c) MAS NMR for NYP-HT-Ar, d) rate performance, e) XPS for NYP-HT- H_2, f) MAS NMR for NYP-HT- H_2, g) correlation of nitrogen species/content and capacitance of various carbons, to note, the detailed N species are based on qualitative analysis combining NMR and XPS, h) ^{1}H-^{15}N 2D NMR for NYP-HT-Ar.

noticeable at 250 ppm, indicating the conversion of unstable N species (part of -NH_2 groups) to more stable aromatic N species[56]. To mention that CP NMR gives very weak signal of N species with H not in proximity[63]. This involves mainly graphitic and pyridinic N. However, these two species play a minor role in our system, showing improved hydrophilicity compared to YP50F in Figure S6, but no influence to our capacitive performance investigation, which will be discussed later.

More interestingly, 2D ^{1}H-^{15}N NMR spectra (Figure 2h and Figure S7) for both NYP-HT-Ar and NYP-HT-H_2 show only one major peak at 10 ppm for ^{1}H signal after the treatment, indicating the conversion of pyridinium N species to pyrrolic N species. These agree well with the XPS result, where a much enhanced pyrrolic signal for both carbons (Figure 2b and 2e) can be observed. Besides, in XPS, the ratio of pyridinic species and graphitic N species also increases for both carbons as they are more thermally stable than -NH_2.

When assembled to supercapacitors in 1 M Li_2SO_4, NYP-HT-Ar shows only a slightly lower capacity versus NYP-HT with even enhanced rate performance in spite of the lowest specific surface area among these three carbons, while NYP-HT-H_2 deteriorates the capacitance back to YP50F level although 3.7 wt% N is maintained (Figure 2d). The different behaviour indicates the nitrogen content is not the only parameter that influences the electrochemical performance, different N species also play a key role. Qualitative analysis (Figure 2g) shows that amine/amide N is directly related to high capacitance. In NYP-HT series, the decreased capacitance is in line with the decreased amine/amide N content, as exemplified by NYP-HT-H_2, with only a small amount of amine/amide N species, showing similar (low) capacitance to undoped YP50F. Besides, pyridinium N also plays an important role. By comparing NYP-HT-Ar and

NYP-HT, there is almost no change in amine/amide groups but all the pyridinium N are converted to pyrrolic N, the capacitance also decreases accordingly, indicating that the pyridinium N is also beneficial for higher capacitance, possibly due to a stronger interaction between the pyridinium N species and anions. As for NYP-HT-H_2, despite 3.7 wt% N (pyrrolic, pyridinic and graphitic N), they have unfortunately no contribution for the capacitance in a neutral aqueous supercapacitor. To the best of our knowledge, this is the first report to distinguish and to clarify the role of pyridinium from pyrrolic N etc. in supercapacitors[9, 28]. Their role should and must be reconsidered and further experiments still need to be done to confirm our findings.

Electrochemical Quartz Crystal Microbalance technique was further used in a gravimetric mode to monitor the ionic fluxes of each carbon electrode during polarization in 1 M Li_2SO_4 aqueous electrolyte. Cyclic voltammograms recorded at 20 $mV{\cdot}s^{-1}$ and the associated frequency change of YP50F and NYP-HT carbons are shown in Figures S8a and b. Both carbons show a typical capacitive behaviour in 1 M Li_2SO_4 aqueous electrolyte, as can be seen from the rectangular shape of the CVs. The motional resistance for the carbon electrodes was stable during polarization (see Figures S8c and d), validating the gravimetric analysis of the frequency change. Small hysteresis was observed in the CV plots (Figure S8a) between positive and negative polarization. However, the starting and ending points in the Δf vs. E plot overlap, which indicates no irreversible mass change occurs after a charge/discharge cycle. The hysteresis is then assumed to come from the difference in adsorption kinetics between cations and anions, such as reported earlier.[64]

Sauerbrey's equation (Eq. 1) was used to calculate the electrode weight change from the frequency change in Figure S8:

$$\Delta m = \frac{-A\sqrt{\mu_q \rho_q}}{2f_0^2}\Delta f = -C_f \Delta f \qquad (1)$$

where ρ_q is the density of quartz (2.648 g cm^{-3}), μ_q is the shear modulus of quartz (2.947 $\times 10^{11}$ g cm s^{-2}), f_o is the fundamental resonance frequency of the quartz and C_f is the calibration constant (or sensitivity factor). The calibration factor was obtained by conducting Cu plating experiment, as detailed in the supplementary information (Figure S9). The C_f was calculated to be 20.24 $ng{\cdot}Hz^{-1}$ (or 15.94 $ng{\cdot}Hz^{-1}cm^{-2}$ taking into account the Au crystal electrode surface of 1.27 cm^2). The change of the electrode weight (Δm) vs. charge (ΔQ) of the carbon electrodes recorded at a potential scan rate of 20 $mV{\cdot}s^{-1}$ are shown in Figure 3c, where the open circuit potential (OCP) was taken as the origin of the plot. It shows an increase of the mass during positive polarization of YP50F carbon, while no or small weight change is observed during negative polarization, limited to a few mC cm^{-2}. The observed weight increase during positive polarization well agrees with a counter ion (anion) adsorption charge storage mechanism.[46, 65] The electrochemical charge storage mechanism is then mainly driven by anion (SO_4^{2-}) adsorption-desorption for (undoped) YP50F microporous carbon. Differently, the electrochemical behaviour of N-doped NYP-HT carbon is mainly driven by cation adsorption-desorption (Li^+), characterized by an increase of weight during negative polarization. It is worth noting a short positive branch, over 1 $mC.cm^{-2}$, is also present, which can be ascribed to anion adsorption-desorption. In summary, the N-doping content not only affects the carbon capacitance but also the charge storage mechanism: for YP50F, anions ensure the charge compensation while for NYP-HT, cations are mainly involved, as can be seen from the electrode weight change during polarization in 1 M Li_2SO_4 aqueous electrolyte.

The origin of the different capacitance values and charge storage mechanism might be the result of the modification of the carbon surface with various nitrogen doping species. To get further insights in their surface chemistry, zeta potential measurements of the different carbons were made in 0.01 M Li_2SO_4 aqueous electrolyte, at pH 7 (Figure S10) and the values are given in Figure 3d. YP50F (undoped) carbon shows a zeta potential of about -5 mV, accounting for the presence of few negatively charged groups and π electron system on the carbon (particle) surface. Whereas the zeta potential of NYP-HT was found to be more negative (~-19 mV), which represents an important change in the surface charge. This suggests the existence of strong anion-carbon interaction for the NYP-HT carbon, resulting in spontaneous chemisorbed-like SO_4^{2-} anions at the carbon surface after immersion in the electrolyte (Figure 3b, 0 V). Zeta potentials and the potential of zero charge (PZC) are strongly related. Different from open circuit potential (OCP), which stands for the rest potential (zero current) of the electrode, PZC represents the potential where the charge on the carbon is null; it defines the border between a region where the negative charge on the carbon surface is balanced with cations for a potential more cathodic (negative) than PZC, while it is the other way around for a potential higher than PZC. As a result, a change in the PZC value of the carbon results in different electrochemical behavior. Therefore, PZCs of the YP50F and NYP-HT carbons were determined from three-electrode cell measurements in 1 M Li_2SO_4 electrolyte (see Figure S11), and the values are given in Figure 3e. PZC of YP50F was found to be more negative (-0.5 V vs

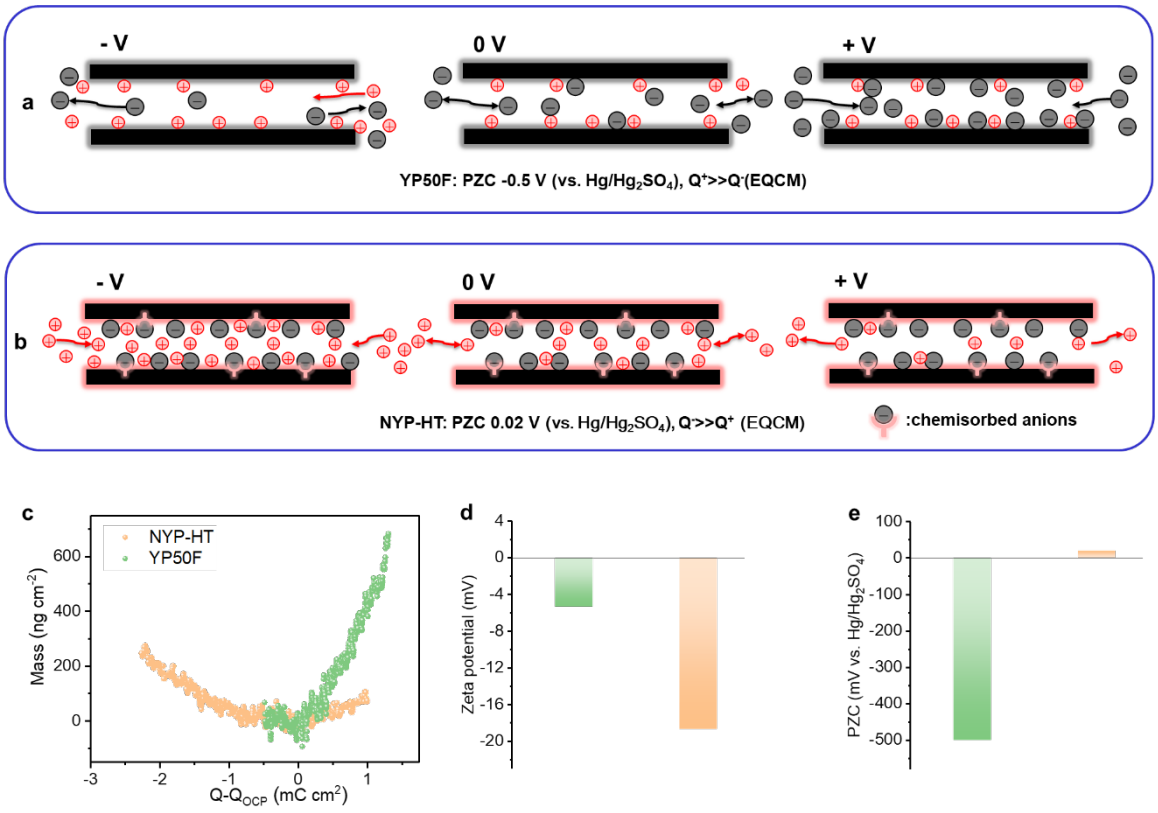

Figure 3. Schematic illustration of possible charging mechanisms of a) YP50F and b) NYP-HT, YP50F prefers adsorbing cations on the surface and anions are probably the main charge carrier and NYP-HT prefers fixing anions on the surface and cations are the main charge carrier, c) Electrode mass vs. charge in 1 M Li_2SO_4 electrolyte calculated during polarization at 20 $mV \cdot s^{-1}$, the origin of the plots (m=0, Q=0) is taken as the open circuit potential, d) zeta potential (measured in 0.01 M Li_2SO_4 aqueous electrolyte) of YP50F (green) and NYP-HT(orange), e)potential of zero charge (PZC, obtained during electrochemical polarization in 1 M Li_2SO_4 electrolyte) for YP50F (green) and NYP-HT(orange).

Hg/Hg_2SO_4) compared to NYP-HT (0.02 V vs Hg/Hg_2SO_4). This is fully consistent with the difference measured in the zeta potentials: a more positive polarization is needed to neutralize the negative charge present on the particle of the NYP-HT carbon, resulting in higher PZC. This can also possibly explain why Li^+ is the main charge carrier for NYP-HT since the SO_4^{2-} ions are specifically adsorbed (immobilized) on the surface and can barely contribute to the charge process (Figure 3b, bottom). Another interesting point is that the shift of the PZC to positive potentials opens the electrochemical polarization window in the negative potential range for NYP-HT carbon, as can be seen in Figure 3c. This is probably the main reason for the enhanced capacitance. Oppositely, the shift of the PZC for YP50F to more negative values compared to NYP-HT reflects more favorable interactions between the carbon surface and the Li^+ ions, making SO_4^{2-} ions the main charge carriers in the charge process (Figure 3a). Additionally, CVs recorded in 3-electrode set-up measurement confirmed the capacitance difference between those two samples, with 112 and 90 F/g measured for NYP-HT and YP50F carbons, respectively. All in all, the N-doping of porous carbons improves the charge storage mechanism: the involved Li^+ ions interact more strongly with the carbon surface and they more concentrated than SO_4^{2-} anions inside pores.

Conclusion

The activated carbon YP50F was used as a model system to study the role of surface N-functionalization by hydrothermal treatment with urea whilst maintaining its porosity. The obtained N-functionalized NYP-HT shows a high nitrogen amount of 4.8 wt% and much improved capacitance (135%) compared to the undoped one as a result of improved hydrophilicity and stronger cation-carbon interaction. Further heating treatment at 773 K under Ar and H_2 atmosphere gives rise to distinctive electrochemical performances, where NYP-HT-Ar still has a high capacitance while NYP-HT-H_2 deteriorates back to the undoped YP50F level. Elemental analysis, X-ray photoelectron spectroscopy and NMR

spectroscopy depict a comprehensive correlation between electrochemical performance and carbon surface chemistry. Rather than the total number of nitrogen, specific N species play a key role in EDLCs. Amine/amide N is found to be the most important species for a high capacitance in a neutral electrolyte while pyridinic N, pyrrolic N and quaternary N show almost no influences. Moreover, the role of pyridinium N is for the first time clearly distinguished and clarified from pyrrolic N with the help of 2D NMR spectroscopy, showing a positive effect for supercapacitor, so far neglected or overlooked in previous reports. Meanwhile, EQCM proves that, the charging mechanism is directed by N doping. Undoped YP50F mainly involves anions adsorption-desorption but for NYP-HT, cations are mainly involved. This could be another reason why NYP-HT has a better capacitance. We hope our study will stimulate studies to investigate a wider variety of electrolytes, like organic and ionic liquid electrolytes to improve the understanding of charge storage mechanisms in high power devices.

SUPPORTING INFORMATION

This material is available free of charge via the Internet at http://pubs.acs.org

AUTHOR INFORMATION

Corresponding Author

Fei Xu: Inorganic Chemistry I, Technische Universität Dresden, Bergstraße 66, 01069 Dresden, Germany; Email: feixu@nwpu.edu.cn

Patrice Simon: Université Paul Sabatier, CIRIMAT UMR CNRS 5085, 31062 Toulouse, France; Réseau sur le Stockage Electrochimique de l'Energie (RS2E), FR CNRS 3459, France; Email : simon@chimie.ups-tlse.fr;

Stefan Kaskel: Inorganic Chemistry I, Technische Universität Dresden, Bergstraße 66, 01069 Dresden, Germany; Fraunhofer Institute for Material and Beam Technology (IWS), Winterbergstraße 28, 01277 Dresden,Germany; Email: stefan.kaskel@tu-dresden.de

ACKNOWLEDGMENT

We thank Steffen Oswald and Lars Giebeler for their XPS measurements. The authors gratefully acknowledge financial support from the German Science Foundation (Deutsche Forschungsgemeinschaft, grants no. KA 1698/27-1).

TOC

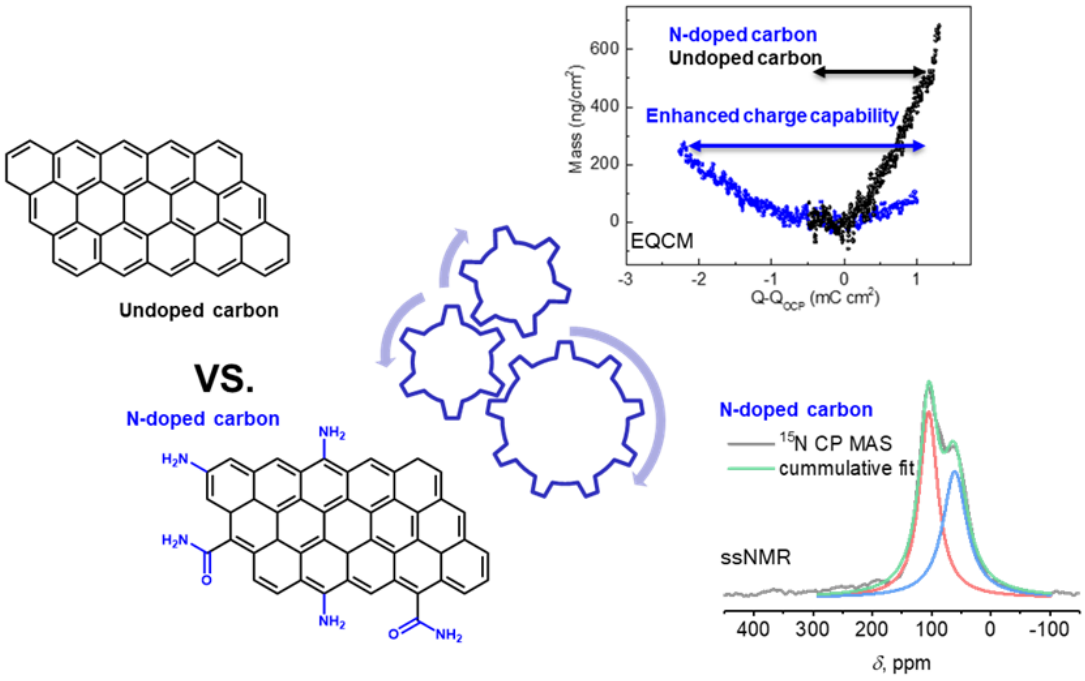
Undoped carbon
VS.
N-doped carbon
N-doped carbon
Undoped carbon
Enhanced charge capability
Mass (ng/cm²)
600
400
200
0
EQCM
-3
-2
-1
0
1
Q-Q_OCP (mC cm²)
N-doped carbon
¹⁵N CP MAS
cummulative fit
ssNMR
400
300
200
100
0
-100
δ, ppm

REFERENCES

1. Simon, P.; Gogotsi, Y., Perspectives for electrochemical capacitors and related devices. *Nat. Mater.* **2020,** *19* (11), 1151-1163.
2. Lin, Z.; Goikolea, E.; Balducci, A.; Naoi, K.; Taberna, P. L.; Salanne, M.; Yushin, G.; Simon, P., Materials for supercapacitors: When Li-ion battery power is not enough. *Mater. Today* **2018,** *21* (4), 419-436.
3. Zhu, Q.; Zhao, D.; Cheng, M.; Zhou, J.; Owusu, K. A.; Mai, L.; Yu, Y., A New View of Supercapacitors: Integrated Supercapacitors. *Adv. Energy Mater.* **2019,** *9* (36), 1901081.
4. Salanne, M.; Rotenberg, B.; Naoi, K.; Kaneko, K.; Taberna, P. L.; Grey, C. P.; Dunn, B.; Simon, P., Efficient storage mechanisms for building better supercapacitors. *Nat. Energy* **2016,** *1* (6), 16070.
5. Zhang, E.; Fulik, N.; Hao, G.-P.; Zhang, H.-Y.; Kaneko, K.; Borchardt, L.; Brunner, E.; Kaskel, S., An Asymmetric Supercapacitor–Diode (CAPode) for Unidirectional Energy Storage. *Angew. Chem. Int. Ed.* **2019,** *58* (37), 13060-13065.
6. Lochmann, S.; Bräuniger, Y.; Gottsmann, V.; Galle, L.; Grothe, J.; Kaskel, S., Switchable Supercapacitors with Transistor-Like Gating Characteristics (G-Cap). *Adv. Funct. Mater.* **2020,** *30* (19), 1910439.
7. Deng, Y.; Xie, Y.; Zou, K.; Ji, X., Review on recent advances in nitrogen-doped carbons: preparations and applications in supercapacitors. *J. Mater. Chem. A* **2016,** *4* (4), 1144-1173.
8. Fic, K.; Płatek, A.; Piwek, J.; Menzel, J.; Ślesiński, A.; Bujewska, P.; Galek, P.; Frąckowiak, E., Revisited insights into charge storage mechanisms in electrochemical capacitors with Li_2SO_4-based electrolyte. *Energy Storage Mater.* **2019,** *22*, 1-14.
9. Wang, H.; Shao, Y.; Mei, S.; Lu, Y.; Zhang, M.; Sun, J.-k.; Matyjaszewski, K.; Antonietti, M.; Yuan, J., Polymer-Derived Heteroatom-Doped Porous Carbon Materials. *Chem. Rev.* **2020,** *120* (17), 9363-9419.
10. Shen, W.; Fan, W., Nitrogen-containing porous carbons: synthesis and application. *J. Mater. Chem. A* **2013,** *1* (4), 999-1013.
11. Benzigar, M. R.; Talapaneni, S. N.; Joseph, S.; Ramadass, K.; Singh, G.; Scaranto, J.; Ravon, U.; Al-Bahily, K.; Vinu, A., Recent advances in functionalized micro and mesoporous carbon materials: synthesis and applications. *Chem. Soc. Rev.* **2018,** *47* (8), 2680-2721.
12. Zhang, E.; Hao, G. P.; Casco, M. E.; Bon, V.; Gratz, S.; Borchardt, L., Nanocasting in ball mills - combining ultra-hydrophilicity and ordered mesoporosity in carbon materials. *J. Mater. Chem. A* **2018,** *6* (3), 859-865.
13. Xiao, K.; Ding, L. X.; Liu, G.; Chen, H.; Wang, S.; Wang, H., Freestanding, hydrophilic nitrogen-doped carbon foams for highly compressible all solid-state supercapacitors. *Adv. Mater.* **2016,** *28* (28), 5997-6002.
14. Ghosh, S.; Barg, S.; Jeong, S. M.; Ostrikov, K., Heteroatom-Doped and Oxygen-Functionalized Nanocarbons for High-Performance Supercapacitors. *Adv. Energy Mater.* **2020,** *10* (32), 2001239.
15. Xiong, Y.; Dong, J.; Huang, Z. Q.; Xin, P.; Chen, W.; Wang, Y.; Li, Z.; Jin, Z.; Xing, W.; Zhuang, Z.; Ye, J.; Wei, X.; Cao, R.; Gu, L.; Sun, S.; Zhuang, L.; Chen, X.; Yang, H.; Chen, C.; Peng, Q.; Chang, C. R.; Wang, D.; Li, Y., Single-atom Rh/N-doped carbon electrocatalyst for formic acid oxidation. *Nat. Nanotechnol.* **2020,** *15* (5), 390-397.
16. Yoo, T. Y.; Yoo, J. M.; Sinha, A. K.; Bootharaju, M. S.; Jung, E.; Lee, H. S.; Lee, B. H.; Kim, J.; Antink, W. H.; Kim, Y. M.; Lee, J.; Lee, E.; Lee, D. W.; Cho, S. P.; Yoo, S. J.; Sung, Y. E.; Hyeon, T., Direct Synthesis of Intermetallic Platinum-Alloy Nanoparticles Highly Loaded on Carbon Supports for Efficient Electrocatalysis. *J. Am. Chem. Soc.* **2020,** *142* (33), 14190-14200.
17. Zhao, D.; Sun, K.; Cheong, W. C.; Zheng, L.; Zhang, C.; Liu, S.; Cao, X.; Wu, K.; Pan, Y.; Zhuang, Z.; Hu, B.; Wang, D.; Peng, Q.; Chen, C.; Li, Y., Synergistically Interactive Pyridinic-N-MoP Sites: Identified Active Centers for Enhanced Hydrogen Evolution in Alkaline Solution. *Angew. Chem. Int. Ed.* **2020,** *59* (23), 8982-8990.
18. Ott, S.; Orfanidi, A.; Schmies, H.; Anke, B.; Nong, H. N.; Hübner, J.; Gernert, U.; Gliech, M.; Lerch, M.; Strasser, P., Ionomer distribution control in porous carbon-supported catalyst layers for high-power and low Pt-loaded proton exchange membrane fuel cells. *Nat. Mater.* **2020,** *19* (1), 77-85.

19. Perovic, M.; Qin, Q.; Oschatz, M., From Molecular Precursors to Nanoparticles—Tailoring the Adsorption Properties of Porous Carbon Materials by Controlled Chemical Functionalization. *Adv. Funct. Mater.* **2020,** *30* (41), 1908371.
20. Matanovic, I.; Artyushkova, K.; Strand, M. B.; Dzara, M. J.; Pylypenko, S.; Atanassov, P., Core Level Shifts of Hydrogenated Pyridinic and Pyrrolic Nitrogen in the Nitrogen-Containing Graphene-Based Electrocatalysts: In-Plane vs Edge Defects. *J. Phys. Chem. C* **2016,** *120* (51), 29225-29232.
21. Lv, R.; Li, Q.; Botello-Méndez, A. R.; Hayashi, T.; Wang, B.; Berkdemir, A.; Hao, Q.; Elías, A. L.; Cruz-Silva, R.; Gutiérrez, H. R.; Kim, Y. A.; Muramatsu, H.; Zhu, J.; Endo, M.; Terrones, H.; Charlier, J.-C.; Pan, M.; Terrones, M., Nitrogen-doped graphene: beyond single substitution and enhanced molecular sensing. *Sci. Rep.* **2012,** *2* (1), 586.
22. Inagaki, M.; Toyoda, M.; Soneda, Y.; Morishita, T., Nitrogen-doped carbon materials. *Carbon* **2018,** *132*, 104-140.
23. Hulicova-Jurcakova, D.; Kodama, M.; Shiraishi, S.; Hatori, H.; Zhu, Z. H.; Lu, G. Q., Nitrogen-Enriched Nonporous Carbon Electrodes with Extraordinary Supercapacitance. *Adv. Funct. Mater.* **2009,** *19* (11), 1800-1809.
24. Lota, G.; Fic, K.; Frackowiak, E., Carbon nanotubes and their composites in electrochemical applications. *Energy Environ. Sci.* **2011,** *4* (5), 1592-1605.
25. Kabir, S.; Artyushkova, K.; Serov, A.; Kiefer, B.; Atanassov, P., Binding energy shifts for nitrogen-containing graphene-based electrocatalysts – experiments and DFT calculations. *Surf. Interface Anal.* **2016,** *48* (5), 293-300.
26. Niwa, H.; Horiba, K.; Harada, Y.; Oshima, M.; Ikeda, T.; Terakura, K.; Ozaki, J.-i.; Miyata, S., X-ray absorption analysis of nitrogen contribution to oxygen reduction reaction in carbon alloy cathode catalysts for polymer electrolyte fuel cells. *J. Power Sources* **2009,** *187* (1), 93-97.
27. Xing, T.; Zheng, Y.; Li, L. H.; Cowie, B. C. C.; Gunzelmann, D.; Qiao, S. Z.; Huang, S.; Chen, Y., Observation of Active Sites for Oxygen Reduction Reaction on Nitrogen-Doped Multilayer Graphene. *ACS Nano* **2014,** *8* (7), 6856-6862.
28. Liu, D.; Ni, K.; Ye, J.; Xie, J.; Zhu, Y.; Song, L., Tailoring the Structure of Carbon Nanomaterials toward High-End Energy Applications. *Adv. Mater.* **2018,** *30* (48), 1802104.
29. Lee, S. H.; Kim, J.; Chung, D. Y.; Yoo, J. M.; Lee, H. S.; Kim, M. J.; Mun, B. S.; Kwon, S. G.; Sung, Y.-E.; Hyeon, T., Design Principle of Fe–N–C Electrocatalysts: How to Optimize Multimodal Porous Structures? *J. Am. Chem. Soc.* **2019,** *141* (5), 2035-2045.
30. Xu, F.; Zhai, Y.; Zhang, E.; Liu, Q.; Jiang, G.; Xu, X.; Qiu, Y.; Liu, X.; Wang, H.; Kaskel, S., Ultrastable Surface-Dominated Pseudocapacitive Potassium Storage Enabled by Edge-Enriched N-Doped Porous Carbon Nanosheets. *Angew. Chem. Int. Ed.* **2020,** *59* (44), 19460-19467.
31. Zhang, E.; Casco, M. E.; Xu, F.; Sheng, W.-B.; Oswald, S.; Giebeler, L.; Wegner, K.; Borchardt, L.; Kaskel, S., On the origin of mesopore collapse in functionalized porous carbons. *Carbon* **2019**.
32. Huo, J.; Duan, P.; Pham, H. N.; Chan, Y. J.; Datye, A. K.; Schmidt-Rohr, K.; Shanks, B. H., Improved hydrothermal stability of Pd nanoparticles on nitrogen-doped carbon supports. *Catal. Sci. Technol.* **2018,** *8* (14), 3548-3561.
33. Pels, J. R.; Kapteijn, F.; Moulijn, J. A.; Zhu, Q.; Thomas, K. M., Evolution of nitrogen functionalities in carbonaceous materials during pyrolysis. *Carbon* **1995,** *33* (11), 1641-1653.
34. Lotsch, B. V.; Döblinger, M.; Sehnert, J.; Seyfarth, L.; Senker, J.; Oeckler, O.; Schnick, W., Unmasking Melon by a Complementary Approach Employing Electron Diffraction, Solid-State NMR Spectroscopy, and Theoretical Calculations—Structural Characterization of a Carbon Nitride Polymer. *Chem. - Eur. J.* **2007,** *13* (17), 4969-4980.
35. Lau, V. W.-h.; Moudrakovski, I.; Botari, T.; Weinberger, S.; Mesch, M. B.; Duppel, V.; Senker, J.; Blum, V.; Lotsch, B. V., Rational design of carbon nitride photocatalysts by identification of cyanamide defects as catalytically relevant sites. *Nat. Commun.* **2016,** *7* (1), 12165.

36. Hu, Y.; Shim, Y.; Oh, J.; Park, S.; Park, S.; Ishii, Y., Synthesis of 13C-,15N-Labeled Graphitic Carbon Nitrides and NMR-Based Evidence of Hydrogen-Bonding Assisted Two-Dimensional Assembly. *Chem. Mater.* **2017,** *29* (12), 5080-5089.
37. Zhang, E.; Fulik, N.; Paasch, S.; Borchardt, L.; Kaskel, S.; Brunner, E., Ionic liquid - Electrode materials interactions studied by NMR spectroscopy, cyclic voltammetry, and impedance spectroscopy. *Energy Storage Mater.* **2019,** *19*, 432-438.
38. Li, X.; Sergeyev, I. V.; Aussenac, F.; Masters, A. F.; Maschmeyer, T.; Hook, J. M., Dynamic Nuclear Polarization NMR Spectroscopy of Polymeric Carbon Nitride Photocatalysts: Insights into Structural Defects and Reactivity. *Angew. Chem. Int. Ed.* **2018,** *57* (23), 6848-6852.
39. Forse, Alexander C.; Griffin, John M.; Merlet, C.; Carretero-Gonzalez, J.; Raji, A.-Rahman O.; Trease, Nicole M.; Grey, Clare P., Direct observation of ion dynamics in supercapacitor electrodes using in situ diffusion NMR spectroscopy. *Nat. Energy* **2017,** *2* (3), 16216.
40. Liu, T.; Leskes, M.; Yu, W.; Moore, A. J.; Zhou, L.; Bayley, P. M.; Kim, G.; Grey, C. P., Cycling Li-O_2 batteries via LiOH formation and decomposition. *Science* **2015,** *350* (6260), 530-533.
41. Leskes, M.; Kim, G.; Liu, T.; Michan, A. L.; Aussenac, F.; Dorffer, P.; Paul, S.; Grey, C. P., Surface-Sensitive NMR Detection of the Solid Electrolyte Interphase Layer on Reduced Graphene Oxide. *J. Phys. Chem. Lett.* **2017,** *8* (5), 1078-1085.
42. Zhao, E. W.; Jónsson, E.; Jethwa, R. B.; Hey, D.; Lyu, D.; Brookfield, A.; Klusener, P. A. A.; Collison, D.; Grey, C. P., Coupled In Situ NMR and EPR Studies Reveal the Electron Transfer Rate and Electrolyte Decomposition in Redox Flow Batteries. *J. Am. Chem. Soc.* **2021,** *143* (4), 1885-1895.
43. Szewczyk, I.; Rokicińska, A.; Michalik, M.; Chen, J.; Jaworski, A.; Aleksis, R.; Pell, A. J.; Hedin, N.; Slabon, A.; Kuśtrowski, P., Electrochemical Denitrification and Oxidative Dehydrogenation of Ethylbenzene over N-doped Mesoporous Carbon: Atomic Level Understanding of Catalytic Activity by 15N NMR Spectroscopy. *Chem. Mater.* **2020,** *32* (17), 7263-7273.
44. Zhang, E.; Fulik, N.; Zhang, H.; Bevilacqua, N.; Zeis, R.; Xu, F.; Brunner, E.; Kaskel, S., NMR analysis of phosphoric acid distribution in porous fuel cell catalysts. *Chem. Commun.* **2021**.
45. Salanne, M.; Rotenberg, B.; Naoi, K.; Kaneko, K.; Taberna, P. L.; Grey, C. P.; Dunn, B.; Simon, P., Efficient storage mechanisms for building better supercapacitors. *Nat. Energy* **2016,** *1*, 16070.
46. Forse, A. C.; Merlet, C.; Griffin, J. M.; Grey, C. P., New Perspectives on the Charging Mechanisms of Supercapacitors. *J. Am. Chem. Soc.* **2016,** *138* (18), 5731-5744.
47. Griffin, J. M.; Forse, A. C.; Tsai, W. Y.; Taberna, P. L.; Simon, P.; Grey, C. P., In situ NMR and electrochemical quartz crystal microbalance techniques reveal the structure of the electrical double layer in supercapacitors. *Nat. Mater.* **2015,** *14* (8), 812-9.
48. Forse, A. C.; Griffin, J. M.; Merlet, C.; Bayley, P. M.; Wang, H.; Simon, P.; Grey, C. P., NMR Study of Ion Dynamics and Charge Storage in Ionic Liquid Supercapacitors. *J. Am. Chem. Soc.* **2015,** *137* (22), 7231-42.
49. Tsai, W.-Y.; Taberna, P.-L.; Simon, P., Electrochemical Quartz Crystal Microbalance (EQCM) Study of Ion Dynamics in Nanoporous Carbons. *J. Am. Chem. Soc.* **2014,** *136* (24), 8722-8728.
50. Ye, J.; Wu, Y.-C.; Xu, K.; Ni, K.; Shu, N.; Taberna, P.-L.; Zhu, Y.; Simon, P., Charge Storage Mechanisms of Single-Layer Graphene in Ionic Liquid. *J. Am. Chem. Soc.* **2019,** *141* (42), 16559-16563.
51. Wu, Y. C.; Ye, J.; Jiang, G.; Ni, K.; Shu, N.; Taberna, P. L.; Zhu, Y.; Simon, P., Electrochemical characterization of single layer graphene / electrolyte interface: effect of solvent on the interfacial capacitance. *Angew. Chem. Int. Ed.* **2021**.
52. Guo, D.; Shibuya, R.; Akiba, C.; Saji, S.; Kondo, T.; Nakamura, J., Active sites of nitrogen-doped carbon materials for oxygen reduction reaction clarified using model catalysts. *Science* **2016,** *351* (6271), 361-365.
53. Moon, I. K.; Lee, J.; Lee, H., Highly qualified reduced graphene oxides: the best

chemical reduction. *Chem. Commun.* **2011,** *47* (34), 9681-9683.
54. MacIntosh, A. R.; Jiang, G.; Zamani, P.; Song, Z.; Riese, A.; Harris, K. J.; Fu, X.; Chen, Z.; Sun, X.; Goward, G. R., Phosphorus and Nitrogen Centers in Doped Graphene and Carbon Nanotubes Analyzed through Solid-State NMR. *J. Phys. Chem. C* **2018,** *122* (12), 6593-6601.
55. Wang, X.; Hou, Z.; Ikeda, T.; Terakura, K., NMR Chemical Shifts of 15N-Bearing Graphene. *J. Phys. Chem. C* **2014,** *118* (25), 13929-13935.
56. Kuroki, S.; Hosaka, Y.; Yamauchi, C., A solid-state NMR study of the carbonization of polyaniline. *Carbon* **2013,** *55*, 160-167.
57. Falco, C.; Sevilla, M.; White, R. J.; Rothe, R.; Titirici, M.-M., Renewable Nitrogen-Doped Hydrothermal Carbons Derived from Microalgae. *ChemSusChem* **2012,** *5* (9), 1834-1840.
58. Stoychev, G. L.; Auer, A. A.; Neese, F., Efficient and Accurate Prediction of Nuclear Magnetic Resonance Shielding Tensors with Double-Hybrid Density Functional Theory. *J. Chem. Theory Comput.* **2018,** *14* (9), 4756-4771.
59. Tian, K.; Wang, J.; Cao, L.; Yang, W.; Guo, W.; Liu, S.; Li, W.; Wang, F.; Li, X.; Xu, Z.; Wang, Z.; Wang, H.; Hou, Y., Single-site pyrrolic-nitrogen-doped sp2-hybridized carbon materials and their pseudocapacitance. *Nat. Commun.* **2020,** *11* (1), 3884.
60. Schmiers, H.; Friebel, J.; Streubel, P.; Hesse, R.; Köpsel, R., Change of chemical bonding of nitrogen of polymeric N-heterocyclic compounds during pyrolysis. *Carbon* **1999,** *37* (12), 1965-1978.
61. Biemolt, J.; Denekamp, I. M.; Slot, T. K.; Rothenberg, G.; Eisenberg, D., Boosting the Supercapacitance of Nitrogen-Doped Carbon by Tuning Surface Functionalities. *ChemSusChem* **2017,** *10* (20), 4018-4024.
62. Yan, J.; Li, S.; Lan, B.; Wu, Y.; Lee, P. S., Rational Design of Nanostructured Electrode Materials toward Multifunctional Supercapacitors. *Adv. Funct. Mater.* **2020,** *30* (2), 1902564.
63. Zhao, L.; Baccile, N.; Gross, S.; Zhang, Y.; Wei, W.; Sun, Y.; Antonietti, M.; Titirici, M.-M., Sustainable nitrogen-doped carbonaceous materials from biomass derivatives. *Carbon* **2010,** *48* (13), 3778-3787.
64. Levi, M. D.; Sigalov, S.; Salitra, G.; Aurbach, D.; Maier, J., The Effect of Specific Adsorption of Cations and Their Size on the Charge-Compensation Mechanism in Carbon Micropores: The Role of Anion Desorption. *ChemPhysChem* **2011,** *12* (4), 854-862.
65. Levi, M. D.; Salitra, G.; Levy, N.; Aurbach, D.; Maier, J., Application of a quartz-crystal microbalance to measure ionic fluxes in microporous carbons for energy storage. *Nat. Mater.* **2009,** *8* (11), 872-875.